Dealuminated Zeolite Y/SnO2 Nanoparticle Hybrid Sensors for Detecting Trace Levels of Propanol as a Lung Cancer Biomarker

Mohit Kumar*, Achraf EL Mohajir, Franck Berger, Marina Raschetti, and Jean-Baptiste Sanchez

Institut FEMTO-ST, UMR CNRS 6174, Université Bourgogne Franche-Comté, 15B Avenue des montboucons, 25030 Besançon, France.

ABSTRACT: Detection of lung cancer biomarkers (LCBs) from exhaled breath in the early stage can lower the mortality of lung cancer. We report a highly sensitive Dealuminated Zeolite Y (DaY)/SnO_2 nanoparticles (NPs) based sensor for the detection of LCBs at low concentrations. The sensing performances were tested with 200 ppb of propanol, formaldehyde, and toluene LCBs at different operating temperatures from 175 °C to 300 °C. The sensor was found to be highly efficient for propanol detection with a remarkable ~ 96 ± 2 % relative response and a fast response time ~10 ± 1 s at 275 °C. The sensor stability was evaluated with multiple loading-deloading cycles with concentrations from 70 to 200 ppb of propanol. The DaY/SnO_2 NPs sensor was stable for multiple detection cycles of LCBs and exhibited a high relative response at 225 °C for concentrations as low as 70 ppb of propanol. The activation energy was calculated for all LCBs and the lowest was measured for propanol at 56.7 kJ/mol. The DaY zeolite plays the role of an excellent catalyst to the dehydration of propanol molecules into propene. A sensing mechanism was also proposed for the DaY/SnO_2 NPs sensor based on the catalytic behavior of the zeolite DaY as well as the role of the activation energy of LCBs on SnO_2 NPs surface.

KEYWORDS: *Lung cancer biomarker sensor, Exhaled breath volatile organic compounds, Propanol, DaY zeolite, SnO_2 nanoparticles.*

1. INTRODUCTION

Lung cancer is a leading cause of death worldwide, with 1.8 million deaths reported in 2020 according to the most recent World Health Organization (WHO) reports[1,2]. Several methods are used for the diagnosis of this respiratory disease, such as chest X-ray, low-dose computer tomography and sputum cytology etc.[3–6]. These methods are usually costly and are used to detect this disease in late-stage cancer patients which is ineffective in reducing the lung cancer mortality. In the study of Pauling *et al*[7], they introduced the detection of Volatile organic compounds (VOCs) in human exhaled breathe and proposed the analysis of exhaled VOCs as a non-invasive method for the diagnosis of lung cancer. Recently, many studies explored the analysis of VOCs found in the exhaled breath for the early diagnosis of lung cancer[8,9]. In fact, the exhaled human breath consists of hundreds of VOCs at very low concentrations (nanomolar/picomolar) along with O_2, N_2, CO_2 and water vapor. The presence of specific VOCs considered as lung cancer biomarkers (LCBs) can serve as an early diagnosis of lung cancer[10,11]. Clinical trial reports of A. Wehinger *et al*[12], M. Koureas *et al*[13] and others[14–16] show among the many VOCs found in exhaled breath, propanol (up to 450 ppb), formaldehyde (up to 1582 ppb) and toluene (up to 30 ppb) were found in the exhaled breath of primary lung cancer patients.

The development of a cost effective, highly sensitive, and reliable sensor that can detect trace level of LCBs (ppb level) from exhaled breath is needed to track early stage of lung cancer. SnO_2 based gas sensors are an appealing choice owing to their high sensitivity, fast response and low cost, however, their lack of selectivity limits their use[17–19]. In the last few years, adding a zeolite to SnO_2 based sensors enhanced the selective detection of VOC due to the zeolite's limited aperture size and their strong catalytic properties[20–22]. The limited aperture size acts as a filter to VOCs with a larger molecular size. On the other hand, the cations give rise to a strong electrostatic field inside the pores and play an important role as a catalyst that helps in the selective adsorption of targeted VOCs[23,24]. Moreover, the dealumination of zeolites increases the cations density and the mesoporous volume without any change in the zeolite's structure[25,26]. The dealumination also supports in the selective adsorption of VOCs on account of changes in the acid catalysis property of zeolite.

S. Wu *et al*[27] studied the dynamic adsorption of toluene, cyclohexane, butyl acetate, methyl ethyl ketone, and propanol on different percentile of dealuminated zeolite Y (DaY) mixed with ZSM-5 (DaY-65%/ZSM-5 and DaY-50%/ZSM-5) and compared the adsorption and desorption

phenomena with pure ZSM-5. The breakthrough time of propanol with DaY-65%/ZSM-5 was found to be less than half of other VOCs as well as lower compared to DaY-50%/ZSM-5 and pure ZSM-5 adsorbents. This can be explained by the fact that the fast transfer of propanol leads to a short local equilibrium time which can be favorable for the development of a fast response sensor. D. G. Lee *et al*[28] studied the adsorption and thermal regeneration (from 50 to 300°C) of acetone and toluene vapors in DaY zeolite. They reported that the breakthrough time of toluene was shorter than acetone and was showing a strong adsorption affinity on the DaY. Moreover, the energy required for the regeneration of acetone increased drastically. While for toluene, the energy required is constant and no distinct reduction of the uptake occurs after several cycles. These observations support the use of DaY for a repeatable LCBs sensor development. Recently, G. Gregis *et al*[29] successfully detected extremely low concentrations of LCBs: propanol (~20 ppb), toluene (~25 ppb) and o-xylene (~5 ppb) using a SnO_2 sensor and a DaY filled micro-preconcentrator. In this work, the authors suggested that propanol can be catalytically decomposed on DaY zeolite acid sites during the desorption at 250°C and leads to its dehydration into propene. This study shows that DaY is a catalytically reactive zeolite that can promote the detection of trace level LCBs. According to the reported literature, DaY represents a suitable adsorbent for the development of a selective LCBs sensor with a fast response, thermally stable and with a good repeatability.

In this work, we developed a low cost, highly sensitive with a fast response time DaY decorated SnO_2 nanoparticles (DaY/SnO_2 NPs) based LCBs sensor for the early diagnosis of lung cancer. Crystalline SnO_2 NPs were synthesized using the sol-gel method and commercial DaY (99.5% pure) zeolite was added using a simple drop casting approach. The responses of the DaY/SnO_2 NPs sensor were measured at different operating temperature ranging from 175 to 300°C for propanol, formaldehyde and toluene LCBs. In addition, the activation energy for each LCB on DaY/SnO_2 NPs was calculated using Arrenius equation to understand the selective sensing behavior. Sensor's repeatability and stability was evaluated in order to conduct a hysteresis study at 225°C for increasing and decreasing LCB concentrations. Gas sensing mechanism based on the zeolite's adsorption characteristics and activation energy is discussed to develop a low cost, portable and highly selective LCBs sensor.

2. EXPERIMENTAL DETAILS

2.1 Samples: SnO_2 NPs: Tin oxide nanoparticles were prepared using the sol-gel method. First, 5.13 g of $SnCl_4$ was mixed in absolute ethanol and stirred for 24 hours. Then as-prepared solution (9.14 g triethylamine mixed in absolute ethanol) was added in the $SnCl_4$ solution very slowly drop by drop in 45 minutes. This mixture was then stirred for ~14 hours resulting in a precipitate named tin-sol. Finally, tin-sol was mixed in 10 mL of ethanol and 10 mL of water and stirred for 4 hours followed by a thermal treatment in the oven at 400°C for 40 hours in order to obtain crystalline SnO_2 NPs.

Zeolite DaY: A commercial hydrophobic dealuminated zeolite Y (DaY), with $Na_2(Al_2Si_{190}O_{384})$ as a chemical formula, was supplied by Degussa. Its particle size is in the range of 1-5 µm. The textural properties were characterized using Ar adsorption-desorption isotherm in our previous work A. El Mohajir *et al*[30]. The BET area, total pore volume, micropore volume, mesopore volume and average pore diameter were estimated at 762 m^2/g, 0.29 cm^3/g, 0.27 cm^3/g, 0.02 cm^3/g and 10.1 Å, respectively.

2.2 Characterizations: The crystalline analysis of SnO_2 NPs and DaY/SnO_2 NPs was done using the X-ray diffraction (D-8 Advance Broker) technique, equipped with CuK_α X-ray source and energy-dispersive 1D detector. The XRD patterns were obtained with a 2θ configuration ranging from 10° to 70° with a step of 0.02°. The crystalline phase was determined based on the Joint Committee on Powder Diffraction Standards (JCPDS) database. Functional groups identification and chemical signature analysis was done using FTIR (PIKE MIRacle single reflection ATR) spectroscopy. Each spectrum was recorded between 400 and 4000 cm^{-1} with a 4 cm^{-1} spectral resolution. The surface morphology was studied using SEM (MEB/SEM Apreo S) characterization technique.

2.3 Sensors and VOC sensing measurement: Schematic of the sensors fabrication steps from (i) to (v) are shown in Figure 1(a) along with the scheme and SEM images of SnO2, DaY and SEM image of DaY/SnO2 hybrid. As-prepared SnO_2 NPs (2 mg) were mixed in 5 ml ethanol and deposited on two commercial sensor platforms Heraeus MSP 632 of size 6.1 mm × 3.2 mm using the drop-cast method with a 3 µl drop. These platforms are equipped with interdigitated electrodes to measure the sensing layer's resistance. A heating coil and a pt-1000 temperature sensor that allow the heating and measurement of the corresponding temperature of the sensing layer are also found on the MSP 632 platforms. After the deposition of SnO_2 NPs, the sensors were kept at room temperature (RT) for 24 hours allowing the evaporation of ethanol and the formation of the sensing film. The DaY zeolite was decorated on one SnO_2 NPs sensor with a 2 µl drop of the solution (10 mg DaY in 5 ml ethanol) and was kept at RT for 15 hours. Thus, SnO_2 NPs and DaY/SnO_2 NPs sensors were prepared for LCBs sensing measurements.

For the LCBs sensing measurements, each sensor was kept in a 500 ml chamber and aged under synthetic air (8% relative humidity at 25 °C) with a flow of 200 ml/min flow rate for 24 hours at 400°C to ensure the stabilization of the sensing film. Same synthetic air was used as carrier gas for the LCBs sensing measurements and their dilution. LCBs

(propanol, formaldehyde, and toluene) vapors were obtained using a permeation oven and the permeation rate was estimated to be 126 ng/min, 200 ng/min and 235 ng/min for propanol, formaldehyde and toluene, respectively. The sensing performances were evaluated at different operating temperatures ranging from 175 to 300°C at different LCBs concentrations (200, 150, 100 and 70 ppb) that were obtained by the fraction of air and LCB.

3. RESULTS AND DISCUSSION

3.1 Structural and Morphological analysis:

The XRD patterns of SnO_2 NPs and DaY/SnO_2 NPs are shown in Figure 1(b). The crystalline phase of SnO_2 was obtained with diffraction peaks at 31.3°, 39.7° and 61.4° corresponding to (101), (200) and (310) lattice planes of rutile-type SnO_2 (JCPDS 41-1445)[31]. The average grain size was estimated at 3.3 ± 0.7 nm using Debye-Scherrer method. The standard phase of DaY-FAU zeolite peaks were identified at 22.4°, 24.4°, 28.3°, 30.8°, 32.4°, 36.8°, 37.5°, 38.8°, 39.6°, 40.8° suggesting that the mixing of SnO_2 NPs and DaY is well-ordered without any external impurity[32]. However, few peaks of DaY cannot be seen clearly due to overlaps with SnO_2 peaks with no significant changes observed on the peaks of SnO_2. This shows that adding DaY didn't affect the crystallinity of the SnO_2. Figure 1(c) shows the FTIR spectra of the SnO_2 NPs and DaY/SnO_2 NPs for further confirmation of their structural properties. In SnO_2 spectrum, only O-Sn-O and Sn-O bands are observed at 614 and 825 cm^{-1}, respectively. Although along with O-Sn-O and Sn-O bands, additional bands of O-H stretching at 1268 and 1636 cm^{-1}, Brønsted acid sites band at 1455 cm^{-1}, CO_2 (from atmosphere) band at 2356 cm^{-1} and –OH stretching band at 3430 cm^{-1} of Si-OH group were observed in DaY/SnO_2. These additional bands correspond to the DaY and indicate a homogenous distribution of the zeolite over SnO_2 NPs. The surface morphology was also studied using SEM technique. The SEM images of SnO_2 NPs (top left) and DaY/SnO_2 NPs hybrid (top right) and DaY (down right) are shown in Figure 1. The average size of SnO_2 NPs is estimated to be below 5 ± 1 nm and the typical size of identical grains of DaY is measured around hundreds of nm. DaY is well decorated over SnO_2 and is regularly distributed throughout the sensing layer.

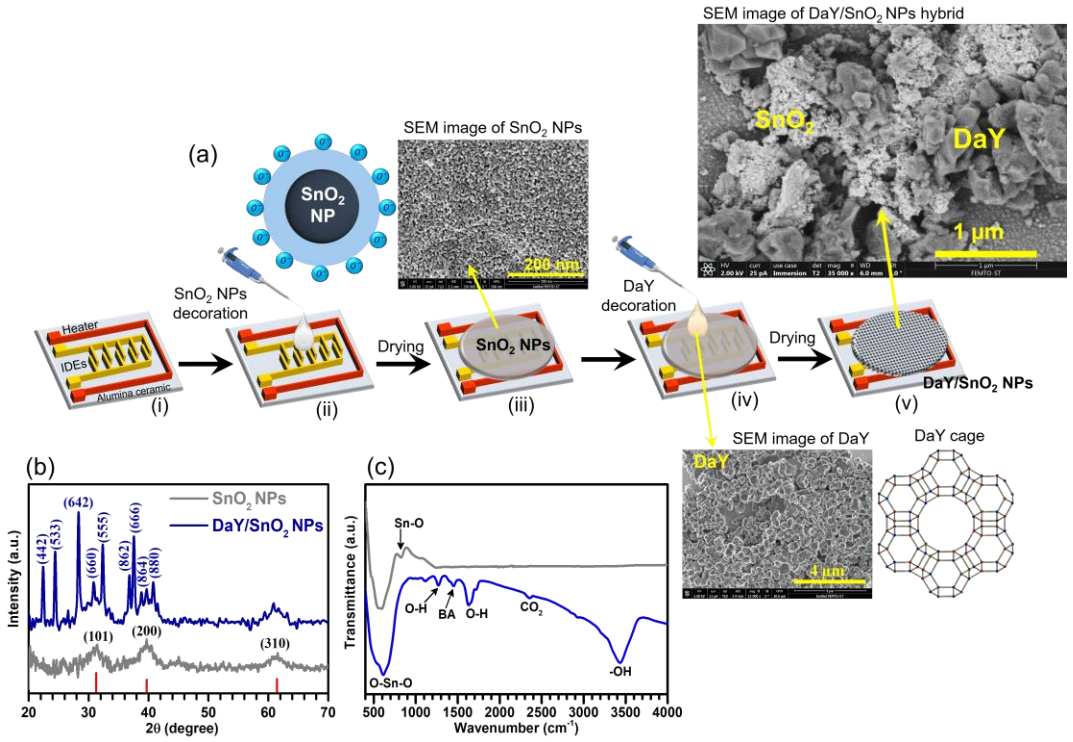

Figure 1. (a) LCB sensor fabrication steps (i) to (iii) are devoted to SnO_2 NPs deposition using the drop cast method on IDEs and heater integrated sensor platform and (iv) and (v) are devoted to DaY decoration on SnO_2 NPs sensor along with the scheme and SEM images of SnO2 and DaY and SEM images of DaY/SnO2 hybrid sensing layer, (b) XRD patterns, and (c) FTIR spectra of SnO_2 NPs and DaY/SnO_2 NPs.

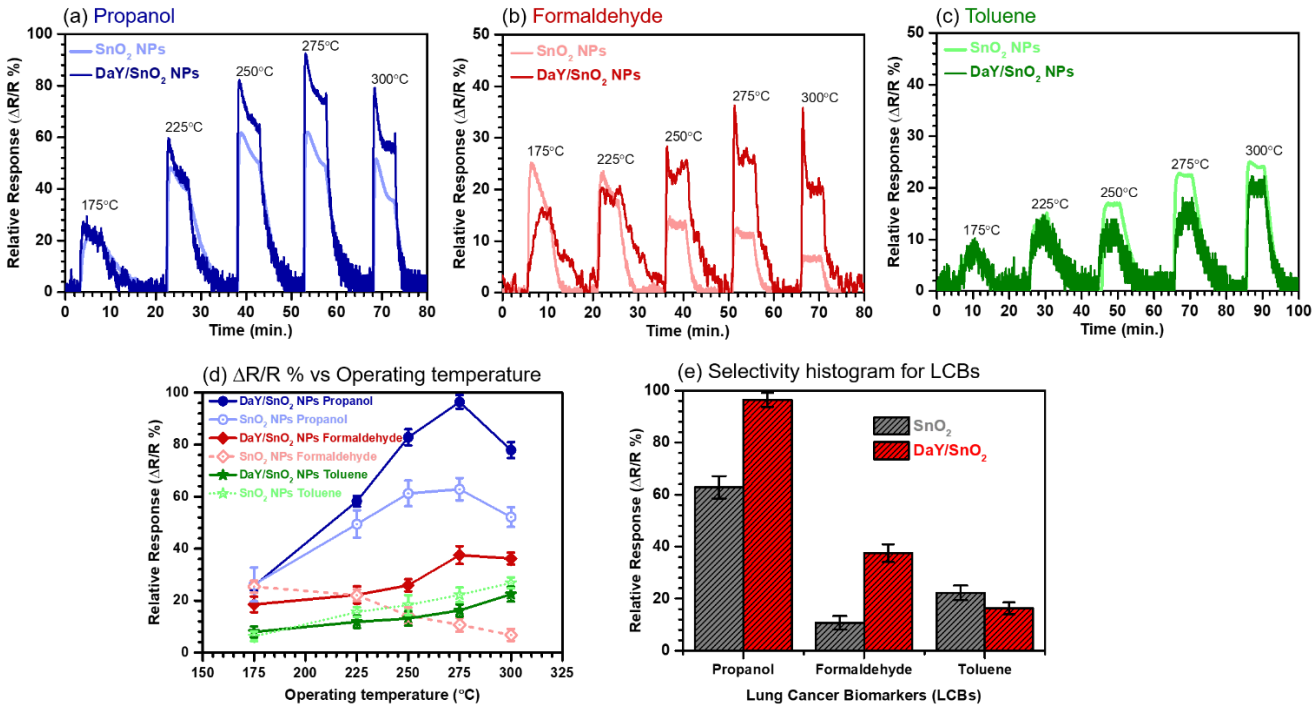

Figure 2. Sensor's relative response curve with time for 200 ppb LCBs (a) Propanol, (b) Formaldehyde and (c) Toluene at operating temperatures between 175 and 300°C, (d) relative response variation with operating temperatures and (e) selectivity histogram for LCBs on SnO_2 and DaY/SnO_2 hydride at 200 ppb and 275 °C operating temperature.

3.2 LCBs Sensing Performance: DaY zeolite is an insulator by nature and works as a size selective adsorbent. The sensing performances are attributed to SnO_2 NPs distribution throughout the sensing layer of DaY/SnO_2. It depends mainly on the reaction of LCBs with chemisorbed oxygen ions species (especially unstable O^-) on the surface of SnO_2 NPs[33,34]. The density of oxygen ions species is highly dependent on the operating temperature. The relative response[35] ($\Delta R/R\ \% = \frac{|R_{air} \sim R_{LCB}|}{R_{air}} \times 100$, where R_{air} is the resistance of sensor in the air and R_{LCB} is the saturated resistance of the sensor after LCB loading in the gas chamber) measurements on SnO_2 NPs and DaY/SnO_2 NPs sensors were done from 175 to 300°C. Figure.2 shows the sensor's relative response curves in respect of time for 200 ppb of (a) propanol, (b) formaldehyde and (c) toluene at different operating temperatures. The time-resistance curves for each LCB at different operating temperatures of both sensors are detailed in the Figure.S1 of the supplementary file. Figure 2(d) summarizes the relative response variation with the operating temperature and Figure 2(e) showing the selectivity histogram for LCBs on SnO_2 and DaY/SnO_2 hydride at 200 ppb and 275 °C operating temperature. The DaY/SnO_2 NPs exhibit an enhanced response for 200 ppb of propanol compared to the SnO_2 NPs sensor. The relative response increases drastically at high temperatures. A relative response of 96.4 ± 2.1 % was observed at 275°C indicating that it's the optimum working temperature. The relative response increases with the operating temperature due to the following reasons: (i) Adsorption of propanol on catalytically active acid sites of the DaY leading to the dehydration of propanol to propene[29,36]. The smaller molecule of propene can then easily diffuse into the porous volume of DaY reacting with oxygen ions species on the surface of SnO_2. With increasing temperatures, the conversion of propanol into propene surges, whereas the dehydration into other products was ceased. (ii) At high temperatures (>150°C), the adsorption of unstable O^- species on SnO_2 NPs surface is more dominating than stable O_2^- and leading the creation of more unstable O^- species[37,38] and leads to an increase of the relative response of DaY/SnO_2 sensor with the operating temperature (96.4 ± 2.1 % at 275°C). As shown in Figure.2 (d), the relative response for propanol is increasing linearly from 175 to 275°C and a slight decrease is observed at 300°C. A similar pattern was found for the SnO_2 NPs sensor. The desorption rate on metal oxide based gas sensor can exceed the adsorption rate after a certain operating temperature[39,40] which can explain the decrease of the relative response of DaY/SnO_2 observed at 300°C. The relative response of the sensor was also recorded for other LCBs, formaldehyde and toluene. For 200 ppb of formaldehyde, it was measured at 18.6 ± 3.0 % at 175°C and increased with higher temperatures with the highest response 37.5 ± 0.5 % recorded at 275°C. The relative response for formaldehyde is lower than the one for propanol due to the conversion of formaldehyde to paraformaldehyde in the DaY cages[41]. The paraformaldehyde molecules are reside in nature inside the main mesopores or inside the secondary micropores of the DaY. The desorption from the zeolite is very slow at low temperatures (<400°C) and

higher temperatures are required for a quick desorption. Thus, a low amount of paraformaldehyde is accessible to react with the oxygen ions on the surface of SnO_2 NPs at operating temperatures in the range of 175 to 275°C which leads to a relatively low response for formaldehyde. On the other hand, the relative response of the SnO_2 NPs sensor is decreasing from 25.4 ± 2.3 % at 175 °C to 6.8 ± 1.7 % at 300°C due to the high desorption rate of formaldehyde on SnO_2 NPs surface[42]. For 200 ppb of toluene, a low relative response of the DaY/SnO_2 NPs sensor (8.0 ± 0.6 %) was recorded at 175°C. The operating tem perature had little to no effect on the sensitivity as 16.3 ± 0.9 % was recorded as a relative response at 250°C. The SnO_2 NPs showed similar performances despite the fact that toluene is strongly affine to adsorb on the DaY and to desorb with short breakthrough time form DaY[28]. In the study of K. Suematsu *et al*[43], it was observed that toluene molecules were insufficiently combusted on the surface of SnO_2 NPs even at 550°C and toluene requires a high activation energy to react with the oxygen species.

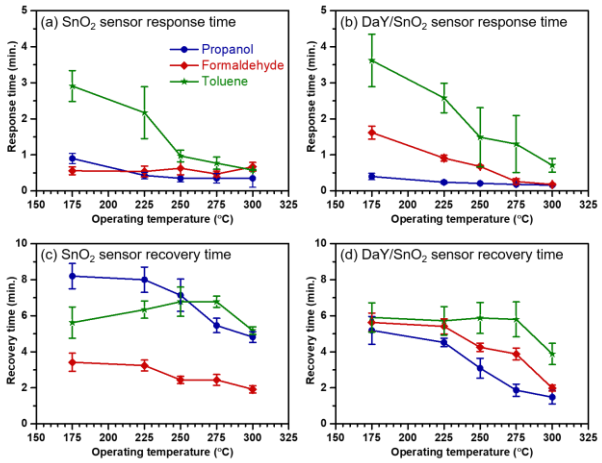

Figure 3. (a) SnO_2 and (b) DaY/SnO_2 sensor response time, and, (a) SnO_2 and (b) DaY/SnO_2 sensor recovery time variation with different operating temperatures for 200 ppb LCBs.

In addition to the relative response, the performances of gas sensors are also evaluated based on its response and recovery times. Figure. 3 shows (a) SnO_2 and (b) DaY/SnO_2 sensor response time, and, (a) SnO_2 and (b) DaY/SnO_2 sensor recovery time with varying temperatures of the DaY/SnO_2 NPs sensor for LCBs. The response and recovery times were calculated as the required times to reach 90% of the saturation value after the exposure to a LBC, and to reach 10% of the saturation value after being exposed to air, respectively[44–46]. For DaY, the response time was found to be decreasing almost linearly with the operating temperature and measured at 0.40 ± 0.09 min. at 175°C, 0.16 ± 0.01 min. (~ 10 s) at 300°C for propanol and found relatively low as compared to SnO_2 sensor. A similar decrease was observed for the other LCBs, from 1.62 ± 0.18 min. at 175°C to 0.18 ± 0.02 min. at 300°C for formaldehyde and 3.62 ± 0.73 min. at 175°C to 0.71 ± 0.19 min. at 300°C for toluene. But it was observed at significant high values as compared to SnO2 sensor. It is happen because addition of porous material (DaY) creates extra disruption in the path of LCBs to reach at SnO_2 surface in the sensor layer. The fast response at high temperatures is a result of the high number of available O^- that are responsible of freeing electrons causing a fast decrease of the resistance of the SnO_2. A similar behavior was observed for the recovery time with increasing temperatures. The recovery time decreased from 5.19 ± 0.77 min. at 175°C to 1.48 ± 0.37 min. (~ 90 s) at 300°C for propanol, from 5.63 ± 0.52 min. at 175°C to 1.98 ± 0.17 min. at 300°C for formaldehyde, and from 5.91 ± 0.81 min. at 175°C to 3.88 ± 0.59 min. at 300°C for toluene. In the comparison of SnO2, the recovery time of DaY/SnO2 for all LCBs shows similar behavior as response time while in the case of toluene it did not change significantly. The relatively high recovery time at low temperatures can be attributed to the inefficient re-adsorption of oxygen ions species on SnO_2 NPs surface.

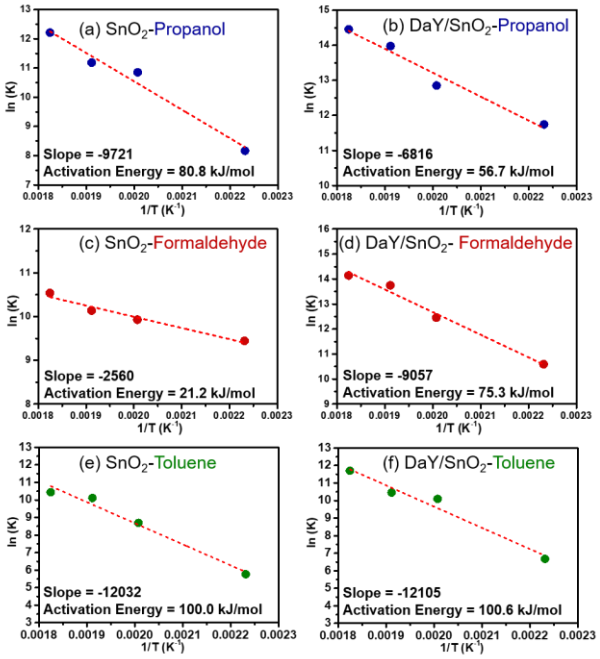

Figure 4. Arrhenius plots of rate of resistance change in respect of temperature for (a), (c) and (d) SnO_2 and (b), (d) and (f) DaY/SnO_2 after 200 ppb exposure of propanol, formaldehyde and toluene, respectively.

Basically, a sensor's performances are highly dependent on the reaction kinetics of LCBs with the oxygen ions species on the surface of SnO_2 NPs that are dependent on the activation energy. The activation energy for each LCB was calculated by applying the Arrhenius equation. Since dimensions and phase of n-type SnO_2 remain the same during the temperature variation, the Arrhenius equation gives the dependence of rate of change in resistance, K, on the absolute temperature T (in kelvin)[48,49]:

$$\ln K = ln\, A_0 - (\Delta E/RT) \qquad (1)$$

A_0 is the pre-exponential factors, ΔE is the activation energy, and R is the gas constant. The resistance's rates of change (K ≈ dR/dt) were evaluated from the variation of the resistance change during a period of time after the exposition to 200 ppb of propanol, formaldehyde and toluene at different operating temperatures. The activation energy for

each LCB was calculated from the slope of Arrhenius plot which is basically a linear fitting of the logarithm of the resistance rate dR/dt in respect to 1/T (K^{-1}). Figure. 4 shows the Arrhenius plot for (a) propanol, (b) formaldehyde and (c) toluene and the calculated values of activation energy were 56.7 kJ/mol for propanol, 75.3 kJ/mol for formaldehyde, and 100.6 kJ/mol for toluene on the DaY/SnO_2 NPs sensing layer. In the comparison of SnO_2, the activation energy for propanol is low, for formaldehyde is high and found very similar for toluene. This observation is in the support of LCBs conversion over DaY zeolite (dehydration of propanol into propene, formaldehyde conversion into paraformaldehyde and, no conversion or no catalytically effect for toluene).

The activation energy for propanol is lower than the other LCBs and our calculated activation energy of DaY/SnO_2 is slightly more as compared to A. Vasile *et al*[50] that reported an activation energy of 34 kJ/mol for propene on SnO_2. This activation energy is very low compared to the activation energies reported by D. Kulkarni *et al*[51] during propanol oxidation on SnO_2 either for redox (96 kJ/mol) or acidic reactions (310 kJ/mol). This implies that the DaY in the sensing layer is playing an active role as a catalyst for the conversion of propanol to propene which leads to good performances in the case of the DaY/SnO_2 sensor. To evaluate the reliability of the DaY/SnO_2 sensor, the stability and repeatability were investigated and are shown in Figure.5. The experiments were conducted at 225 °C with decreasing and increasing concentrations of propanol in order to test the reversibility and repeatability. The sensor showed good repeatability and as expected, the amplitude of the relative response decreases with decreasing concentration from 63.2 ± 6.1 % at 200 ppb to 29.2 ± 5.5 % at 70 ppb (see Figure.5 (b)). Similarly, the response and recovery times (see Figure.5 (c)) of the sensor decreased with lower concentrations. This shows that the DaY/SnO_2 sensor is exhibiting an excellent stability and repeatability to different concentrations of propanol which makes it a reliable sensor for the detection of LCBs from lung cancer patients.

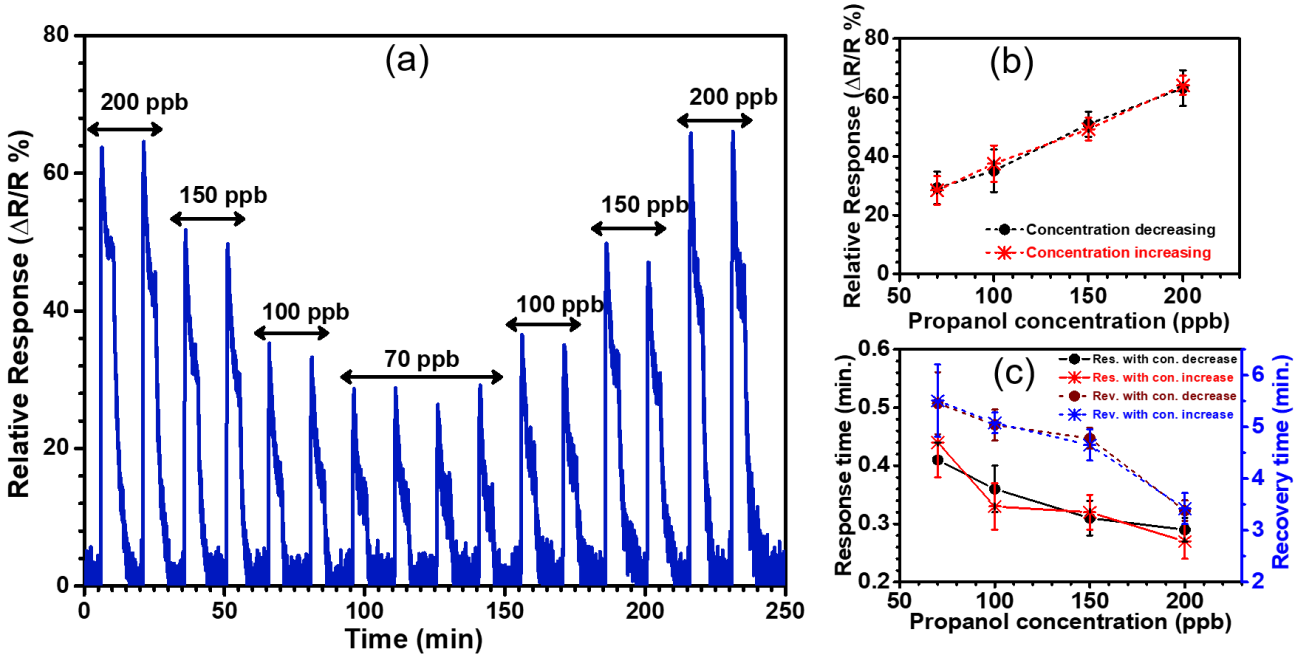

Figure 5. (a) Hysteresis study for propanol, (b) relative response, and (c) response time and recovery time at 225 °C with decreasing and increasing propanol concentrations.

3.3 LCBs-Sensing Mechanism: The LCBs sensing mechanism on the DaY/SnO_2 NPs is mainly influenced by (i) the catalytic conversion and diffusion of gas phase LCBs through the zeolite, and (ii) the activation energy required for LCBs to react with oxygen ions on SnO_2 NPs surface. When propanol molecules interact with DaY at high temperatures, these molecules are catalytically converted into propene through its dehydration over acidic sites of the zeolite according to the steps presented in figure 6 (a)[29]. On the other hand, formaldehyde molecules are trapped in the DaY cages as they form paraformaldehyde[41] and are unable to desorb completely from the zeolite. Moreover, toluene molecules exhibit a high affinity towards DaY, but they require a high activation energy to react with the oxygen ions on SnO_2 NPs surface. As reported in several studies, in the presence of synthetic air, the oxygen ions species (O^-, O^{2-} and O_2^-) are chemisorbed leading to the creation of a depletion region at the surface of SnO_2 NPs[17–19,37,43,52]. These oxygen ions are totally dependent on the operating temperature and at high temperature (>150°C), unstable O^- ions are the dominant oxygen species. When LCBs react

with O^- ions, the trapped electron is released into the conduction region causing a decrease of the width of the depletion region of the SnO2 NPs. Figure.6 (b)-(e) shows a schematic of the relative change in the depletion region of SnO_2 NPs in the presence of (b) synthetic air and of LBCs (c) propene (following the dehydration of propanol), (d) formaldehyde and (e) toluene with their combustion into CO_2 and H_2O. For n-type SnO_2, propene molecules react with adsorbed O^- ions and release electrons. These reactions are the main cause of the decrease in the resistance of SnO_2 while the sensor is exposed to LCBs. Due to the low activation energy required for propene to react with O^- ions compared to formaldehyde and toluene, the DaY/SnO_2 sensor exhibits a high response for propene with the maximum change in the depletion region. Another important factor governing the interaction of LCBs with the sensing material is the operating temperature. The density of chemisorbed O^- ions on the surface of SnO_2 NPs increases with higher operating temperatures and leads to a large change in the depletion region causing an increase of the sensor's resistance. A high sensitivity is then observed due to the higher density of O^- ions interacting with the LCB molecules causing a decrease of the sensor's resistance.

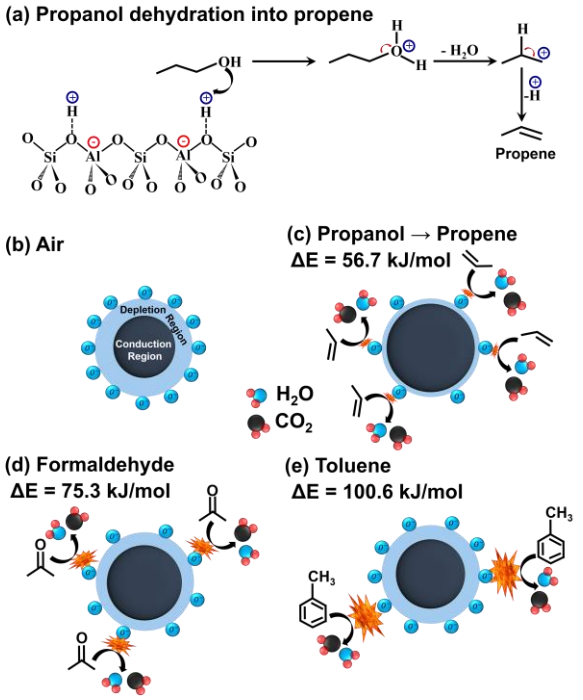

Figure 6. a) Propanol dehydration steps over DaY zeolite acid sites, and the gas sensing mechanism for sensor with a relative change in depletion region of SnO2 NPs in presence of (b) Air, (c) Propanol → Propene, (d) Formaldehyde, and (e) Toluene.

4. CONCLUSIONS

For the early diagnosis of lung cancer from exhaled human breath, a cost-effective DaY/SnO_2 NPs sensor was able to detect extremely low concentrations of LCBs with a high response. Moreover, DaY/SnO_2 NPs sensor showed remarkable enhanced sensing response ~ 96 % for 200 ppb propanol at 275 °C with a record rapid detection time ~10 s. This miniaturized sensor was found to be stable with repeatable detection cycles of LCBs at different concentrations and temperatures. The LCBs sensing mechanism for DaY/SnO_2 NPs sensor was also proposed and is mainly attributed to the zeolite's catalytic role and to the activation energy of reactive LBCs. Indeed, DaY/SnO_2 NPS showed great sensitivity towards LCBs. In conclusion, this work introduced a cheap, efficient, non-invasive and portable device for the diagnosis of early-stage lung cancer.

AUTHOR INFORMATION

Corresponding Author

Mohit Kumar – Institut FEMTO-ST, UMR 6174 CNRS, Université de Bourgogne–Franche-Comté, 25030 Besançon Cedex, France;
Phone: +33 3 63 08 24 88; Email: mohit.kumar@femto-st.fr
orcid.org/0000-0003-0305-7427

Authors

Achraf El Mohajir – *Institut FEMTO-ST, UMR 6174 CNRS, Université de Bourgogne–Franche-Comté, 25030 Besançon*
Franck Berger – *Institut FEMTO-ST, UMR 6174, Université de Bourgogne – Franche-Comté, France*
Marina Raschetti – *Institut FEMTO-ST, UMR 6174 CNRS, Université de Bourgogne–Franche-Comté, 25030 Besançon*
Jean-Baptiste Sanchez – *Institut FEMTO-ST, UMR 6174 CNRS, Université de Bourgogne–Franche-Comté, 25030 Besançon*

Author Contributions

M. Kumar synthesized SnO_2 nanoparticles and did the LCBs sensing experiments, analyzed the data and designed the figures. A. El Mohajir continuously supported in the gas sensing experiments and figure designs. M. Raschetti carried out the SEM analysis. F. Berger provided expertise and feedback. J. B. Sanchez supervised the project, analyzed the data and was in-charge of overall direction and planning. All authors contributed to the interpretation of the results, discussion and writing of the manuscript. All authors gave their approval to the final version of the manuscript.

ACKNOWLEDGMENT

The authors would like to express their gratitude to the Bourgogne Franche-Comté Region, the European fund FEDER, and the EUR EIPHI (contract ANR-17-EURE-0002) for financial support through the project DECOLAIR.

REFERENCES

(1) Siegel, R. L.; Miller, K. D.; Jemal, A. Cancer Statistics, 2020. CA A Cancer J Clin 2020, 70 (1), 7–30. https://doi.org/10.3322/caac.21590.

(2) Cancer https://www.who.int/news-room/fact-sheets/detail/cancer.

(3) Blandin Knight, S.; Crosbie, P. A.; Balata, H.; Chudziak, J.; Hussell, T.; Dive, C. Progress and Prospects of

Early Detection in Lung Cancer. Open Biology 7 (9), 170070. https://doi.org/10.1098/rsob.170070.

(4) Wender, R.; Fontham, E. T. H.; Barrera Jr, E.; Colditz, G. A.; Church, T. R.; Ettinger, D. S.; Etzioni, R.; Flowers, C. R.; Scott Gazelle, G.; Kelsey, D. K.; LaMonte, S. J.; Michaelson, J. S.; Oeffinger, K. C.; Shih, Y.-C. T.; Sullivan, D. C.; Travis, W.; Walter, L.; Wolf, A. M. D.; Brawley, O. W.; Smith, R. A. American Cancer Society Lung Cancer Screening Guidelines. CA: A Cancer Journal for Clinicians 2013, 63 (2), 106–117. https://doi.org/10.3322/caac.21172.

(5) Ardila, D.; Kiraly, A. P.; Bharadwaj, S.; Choi, B.; Reicher, J. J.; Peng, L.; Tse, D.; Etemadi, M.; Ye, W.; Corrado, G.; Naidich, D. P.; Shetty, S. End-to-End Lung Cancer Screening with Three-Dimensional Deep Learning on Low-Dose Chest Computed Tomography. Nat Med 2019, 25 (6), 954–961. https://doi.org/10.1038/s41591-019-0447-x.

(6) Sands, J.; Tammemägi, M. C.; Couraud, S.; Baldwin, D. R.; Borondy-Kitts, A.; Yankelevitz, D.; Lewis, J.; Grannis, F.; Kauczor, H.-U.; von Stackelberg, O.; Sequist, L.; Pastorino, U.; McKee, B. Lung Screening Benefits and Challenges: A Review of The Data and Outline for Implementation. Journal of Thoracic Oncology 2021, 16 (1), 37–53. https://doi.org/10.1016/j.jtho.2020.10.127.

(7) Pauling, L.; Robinson, A. B.; Teranishi, R.; Cary, P. Quantitative Analysis of Urine Vapor and Breath by Gas-Liquid Partition Chromatography. PNAS 1971, 68 (10), 2374–2376. https://doi.org/10.1073/pnas.68.10.2374.

(8) Capuano, R.; Santonico, M.; Pennazza, G.; Ghezzi, S.; Martinelli, E.; Roscioni, C.; Lucantoni, G.; Galluccio, G.; Paolesse, R.; Di Natale, C.; D'Amico, A. The Lung Cancer Breath Signature: A Comparative Analysis of Exhaled Breath and Air Sampled from inside the Lungs. Sci Rep 2015, 5 (1), 16491. https://doi.org/10.1038/srep16491.

(9) Gashimova, E.; Osipova, A.; Temerdashev, A.; Porkhanov, V.; Polyakov, I.; Perunov, D.; Dmitrieva, E. Exhaled Breath Analysis Using GC-MS and an Electronic Nose for Lung Cancer Diagnostics. Anal. Methods 2021, 13 (40), 4793–4804. https://doi.org/10.1039/D1AY01163D.

(10) Broza, Y. Y.; Mochalski, P.; Ruzsanyi, V.; Amann, A.; Haick, H. Hybrid Volatolomics and Disease Detection. Angewandte Chemie International Edition 2015, 54 (38), 11036–11048. https://doi.org/10.1002/anie.201500153.

(11) Amann, A.; Costello, B. de L.; Miekisch, W.; Schubert, J.; Buszewski, B.; Pleil, J.; Ratcliffe, N.; Risby, T. The Human Volatilome: Volatile Organic Compounds (VOCs) in Exhaled Breath, Skin Emanations, Urine, Feces and Saliva. J. Breath Res. 2014, 8 (3), 034001. https://doi.org/10.1088/1752-7155/8/3/034001.

(12) Wehinger, A.; Schmid, A.; Mechtcheriakov, S.; Ledochowski, M.; Grabmer, C.; Gastl, G. A.; Amann, A. Lung Cancer Detection by Proton Transfer Reaction Mass-Spectrometric Analysis of Human Breath Gas. International Journal of Mass Spectrometry 2007, 265 (1), 49–59. https://doi.org/10.1016/j.ijms.2007.05.012.

(13) Koureas, M.; Kirgou, P.; Amoutzias, G.; Hadjichristodoulou, C.; Gourgoulianis, K.; Tsakalof, A. Target Analysis of Volatile Organic Compounds in Exhaled Breath for Lung Cancer Discrimination from Other Pulmonary Diseases and Healthy Persons. Metabolites 2020, 10 (8), 317. https://doi.org/10.3390/metabo10080317.

(14) Ligor, M.; Ligor, T.; Bajtarevic, A.; Ager, C.; Pienz, M.; Klieber, M.; Denz, H.; Fiegl, M.; Hilbe, W.; Weiss, W.; Lukas, P.; Jamnig, H.; Hackl, M.; Buszewski, B.; Miekisch, W.; Schubert, J.; Amann, A. Determination of Volatile Organic Compounds in Exhaled Breath of Patients with Lung Cancer Using Solid Phase Microextraction and Gas Chromatography Mass Spectrometry. Clinical Chemistry and Laboratory Medicine 2009, 47 (5), 550–560. https://doi.org/10.1515/CCLM.2009.133.

(15) Fuchs, P.; Loeseken, C.; Schubert, J. K.; Miekisch, W. Breath Gas Aldehydes as Biomarkers of Lung Cancer. International Journal of Cancer 2010, 126 (11), 2663–2670. https://doi.org/10.1002/ijc.24970.

(16) Dent, A. G.; Sutedja, T. G.; Zimmerman, P. V. Exhaled Breath Analysis for Lung Cancer. Journal of Thoracic Disease 2013, 5 (5). https://doi.org/10.3978/j.issn.2072-1439.2013.08.44.

(17) Kang, X.; Deng, N.; Yan, Z.; Pan, Y.; Sun, W.; Zhang, Y. Resistive-Type VOCs and Pollution Gases Sensor Based on SnO_2: A Review. Materials Science in Semiconductor Processing 2022, 138, 106246. https://doi.org/10.1016/j.mssp.2021.106246.

(18) Li, Z.; Zhao, Q.; Fan, W.; Zhan, J. Porous SnO2 Nanospheres as Sensitive Gas Sensors for Volatile Organic Compounds Detection. Nanoscale 2011, 3 (4), 1646–1652. https://doi.org/10.1039/CoNR00728E.

(19) Acharyya, S.; Jana, B.; Nag, S.; Saha, G.; Guha, P. K. Single Resistive Sensor for Selective Detection of Multiple VOCs Employing SnO_2 Hollowspheres and Machine Learning Algorithm: A Proof of Concept. Sensors and Actuators B: Chemical 2020, 321, 128484. https://doi.org/10.1016/j.snb.2020.128484.

(20) Broek, J. van den; Weber, I. C.; Güntner, A. T.; Pratsinis, S. E. Highly Selective Gas Sensing Enabled by Filters. Mater. Horiz. 2021, 8 (3), 661–684. https://doi.org/10.1039/DoMH01453B.

(21) Hernández, P. T.; Hailes, S. M. V.; Parkin, I. P. Cocaine By-Product Detection with Metal Oxide Semiconductor Sensor Arrays. RSC Adv. 2020, 10 (47), 28464–28477. https://doi.org/10.1039/DoRA03687K.

(22) Sun, Y.; Wang, J.; Li, X.; Du, H.; Huang, Q.; Wang, X. The Effect of Zeolite Composition and Grain Size on Gas Sensing Properties of SnO2/Zeolite Sensor. Sensors 2018, 18 (2), 390. https://doi.org/10.3390/s18020390.

(23) Valdés, H.; Riquelme, A. L.; Solar, V. A.; Azzolina-Jury, F.; Thibault-Starzyk, F. Removal of Chlorinated Volatile Organic Compounds onto Natural and Cu-Modified Zeolite: The Role of Chemical Surface Characteristics in the Adsorption Mechanism. Separation and Purification Technology 2021, 258, 118080. https://doi.org/10.1016/j.seppur.2020.118080.

(24) Wales, D. J.; Grand, J.; Ting, V. P.; Burke, R. D.; Edler, K. J.; Bowen, C. R.; Mintova, S.; Burrows, A. D. Gas

Sensing Using Porous Materials for Automotive Applications. Chem. Soc. Rev. 2015, 44 (13), 4290–4321. https://doi.org/10.1039/C5CS00040H.

(25) de Fonseca, B.; Rossignol, J.; Bezverkhyy, I.; Bellat, J. P.; Stuerga, D.; Pribetich, P. Detection of VOCs by Microwave Transduction Using Dealuminated Faujasite DAY Zeolites as Gas Sensitive Materials. Sensors and Actuators B: Chemical 2015, 213, 558–565. https://doi.org/10.1016/j.snb.2015.02.006.

(26) Hessou, E. P.; Bédé, L. A.; Jabraoui, H.; Semmeq, A.; Badawi, M.; Valtchev, V. Adsorption of Toluene and Water over Cationic-Exchanged Y Zeolites: A DFT Exploration. Molecules 2021, 26 (18), 5486. https://doi.org/10.3390/molecules26185486.

(27) Wu, S.; Wang, Y.; Sun, C.; Zhao, T.; Zhao, J.; Wang, Z.; Liu, W.; Lu, J.; Shi, M.; Zhao, A.; Bu, L.; Wang, Z.; Yang, M.; Zhi, Y. Novel Preparation of Binder-Free Y/ZSM-5 Zeolite Composites for VOCs Adsorption. Chemical Engineering Journal 2021, 417, 129172. https://doi.org/10.1016/j.cej.2021.129172.

(28) Lee, D.-G.; Kim, J.-H.; Lee, C.-H. Adsorption and Thermal Regeneration of Acetone and Toluene Vapors in Dealuminated Y-Zeolite Bed. Separation and Purification Technology 2011, 77 (3), 312–324. https://doi.org/10.1016/j.seppur.2010.12.022.

(29) Gregis, G.; Sanchez, J.-B.; Bezverkhyy, I.; Guy, W.; Berger, F.; Fierro, V.; Bellat, J.-P.; Celzard, A. Detection and Quantification of Lung Cancer Biomarkers by a Micro-Analytical Device Using a Single Metal Oxide-Based Gas Sensor. Sensors and Actuators B: Chemical 2018, 255, 391–400. https://doi.org/10.1016/j.snb.2017.08.056.

(30) El Mohajir, A.; Castro-Gutiérrez, J.; Canevesi, R. L. S.; Bezverkhyy, I.; Weber, G.; Bellat, J.-P.; Berger, F.; Celzard, A.; Fierro, V.; Sanchez, J.-B. Novel Porous Carbon Material for the Detection of Traces of Volatile Organic Compounds in Indoor Air. ACS Appl. Mater. Interfaces 2021, 13 (33), 40088–40097. https://doi.org/10.1021/acsami.1c10430.

(31) Cojocaru, L.; Olivier, C.; Toupance, T.; Sellier, E.; Hirsch, L. Size and Shape Fine-Tuning of SnO2 Nanoparticles for Highly Efficient and Stable Dye-Sensitized Solar Cells. J. Mater. Chem. A 2013, 1 (44), 13789–13799. https://doi.org/10.1039/C3TA12279D.

(32) Parise, J. B.; Corbin, D. R.; Abrams, L.; Cox, D. E. Structure of Dealuminated Linde Y-Zeolite; $Si_{139.7}Al_{52.3}O_{384}$ and $Si_{173.1}Al_{18.9}O_{384}$: Presence of Non-Framework Al Species. Acta Cryst C 1984, 40 (9), 1493–1497. https://doi.org/10.1107/S0108270184008490.

(33) Li, Y.; Luo, N.; Zhang, W.; Hu, Q.; Wang, X.; Chen, Y.; Cheng, Z.; Xu, J. Rational Design and in Situ Growth of SnO_2/CMF Composites: Insightful Understanding of the Formaldehyde Gas Sensing Mechanism and Enhanced Gas Sensing Properties. J. Mater. Chem. C 2020, 8 (36), 12418–12426. https://doi.org/10.1039/D0TC01650K.

(34) Degler, D.; Wicker, S.; Weimar, U.; Barsan, N. Identifying the Active Oxygen Species in SnO_2 Based Gas Sensing Materials: An Operando IR Spectrsocopy Study. J. Phys. Chem. C 2015, 119 (21), 11792–11799. https://doi.org/10.1021/acs.jpcc.5b04082.

(35) Kumar, M.; Kumar, R.; Rajamani, S.; Ranwa, S.; Fanetti, M.; Valant, M.; Kumar, M. Efficient Room Temperature Hydrogen Sensor Based on UV-Activated ZnO Nano-Network. Nanotechnology 2017, 28 (36), 365502. https://doi.org/10.1088/1361-6528/aa7cad.

(36) Triantafillidis, C. S.; Evmiridis, N. P. Dealuminated H–Y Zeolites: Influence of the Number and Type of Acid Sites on the Catalytic Activity for Isopropanol Dehydration. Ind. Eng. Chem. Res. 2000, 39 (9), 3233–3240. https://doi.org/10.1021/ie000002s.

(37) Sopiha, K. V.; Malyi, O. I.; Persson, C.; Wu, P. Chemistry of Oxygen Ionosorption on SnO_2 Surfaces. ACS Appl. Mater. Interfaces 2021, 13 (28), 33664–33676. https://doi.org/10.1021/acsami.1c08236.

(38) Oviedo, J.; Gillan, M. J. First-Principles Study of the Interaction of Oxygen with the SnO_2(110) Surface. Surface Science 2001, 490 (3), 221–236. https://doi.org/10.1016/S0039-6028(01)01372-3.

(39) Lontio Fomekong; Saruhan. Influence of Humidity on NO_2-Sensing and Selectivity of Spray-CVD Grown ZnO Thin Film above 400 °C. Chemosensors 2019, 7 (3), 42. https://doi.org/10.3390/chemosensors7030042.

(40) Wang, C.; Yin, L.; Zhang, L.; Xiang, D.; Gao, R. Metal Oxide Gas Sensors: Sensitivity and Influencing Factors. Sensors 2010, 10 (3), 2088–2106. https://doi.org/10.3390/s100302088.

(41) Bellat, J.-P.; Bezverkhyy, I.; Weber, G.; Royer, S.; Averlant, R.; Giraudon, J.-M.; Lamonier, J.-F. Capture of Formaldehyde by Adsorption on Nanoporous Materials. Journal of Hazardous Materials 2015, 300, 711–717. https://doi.org/10.1016/j.jhazmat.2015.07.078.

(42) Gao, L.; Fu, H.; Zhu, J.; Wang, J.; Chen, Y.; Liu, H. Synthesis of SnO_2 Nanoparticles for Formaldehyde Detection with High Sensitivity and Good Selectivity. Journal of Materials Research 2020, 35 (16), 2208–2217. https://doi.org/10.1557/jmr.2020.181.

(43) Suematsu, K.; Oyama, T.; Mizukami, W.; Hiroyama, Y.; Watanabe, K.; Shimanoe, K. Selective Detection of Toluene Using Pulse-Driven SnO_2 Micro Gas Sensors. ACS Appl. Electron. Mater. 2020, 2 (9), 2913–2920. https://doi.org/10.1021/acsaelm.0c00547.

(44) Yu, H.; Yang, T.; Zhao, R.; Xiao, B.; Li, Z.; Zhang, M. Fast Formaldehyde Gas Sensing Response Properties of Ultrathin SnO_2 Nanosheets. RSC Adv. 2015, 5 (126), 104574–104581. https://doi.org/10.1039/C5RA22755K.

(45) Kumar, M.; Bhati, V. S.; Kumar, M. Effect of Schottky Barrier Height on Hydrogen Gas Sensitivity of Metal/TiO_2 Nanoplates. International Journal of Hydrogen Energy 2017, 42 (34), 22082–22089. https://doi.org/10.1016/j.ijhydene.2017.07.144.

(46) Wang, P.; Yuan, T.; Yuan, H.; Zheng, X.; Ijaz, H.; Hui, J.; Fan, D.; Zhao, Y.; Hu, S. PdO/SnO_2 Heterostructure for Low-Temperature Detection of CO with Fast Response

and Recovery. RSC Adv. 2019, 9 (40), 22875–22882. https://doi.org/10.1039/C9RA03171E.

(47) Kucharski, S.; Blackman, C. Atomistic Descriptions of Gas-Surface Interactions on Tin Dioxide. Chemosensors 2021, 9 (9), 270. https://doi.org/10.3390/chemosensors9090270.

(48) Kumar, M.; Singh Bhati, V.; Ranwa, S.; Singh, J.; Kumar, M. Pd/ZnO Nanorods Based Sensor for Highly Selective Detection of Extremely Low Concentration Hydrogen. Sci Rep 2017, 7 (1), 236. https://doi.org/10.1038/s41598-017-00362-x.

(49) Song, P.; Qin, H.; Huang, S.; Liu, X.; Zhang, R.; Hu, J.; Jiang, M. Characteristics and Sensing Properties of $La_{0.8}Pb_{0.2}Fe_{1-x}Ni_xO_3$ System for CO Gas Sensors. Materials Science and Engineering: B 2007, 138 (2), 193–197. https://doi.org/10.1016/j.mseb.2006.11.022.

(50) Vasile, A.; Caldararu, M.; Hornoiu, C.; Bratan, V.; Ionescu, N. I.; Yuzhakova, T.; Redey, A. ELIMINATION OF GAS POLLUTANTS USING SnO_2-CeO_2 CATALYSTS. Environ. Eng. Manag. J. 2012, 11 (2), 481–485. https://doi.org/10.30638/eemj.2012.060.

(51) Kulkarni, D.; Wachs, I. E. Isopropanol Oxidation by Pure Metal Oxide Catalysts: Number of Active Surface Sites and Turnover Frequencies. Applied Catalysis A: General 2002, 237 (1), 121–137. https://doi.org/10.1016/S0926-860X(02)00325-3.

(52) Sanchez, J.-B.; Sanchez-Sanchez, A.; Izquierdo, M. T.; Mathieu, S.; Ghanbaja, J.; Berger, F.; Celzard, A.; Fierro, V. Nanostructured Tin Oxide Materials for the Sub-Ppm Detection of Indoor Formaldehyde Pollution. Talanta 2020, 208, 120396. https://doi.org/10.1016/j.talanta.2019.120396.

Table of Contents (TOC) graphic